Electronic Supplementary Information

Five-Ring-Fused Asymmetric Thienoacenes for High Mobility Organic Thin-Film Transistors: the Influence of the Position of S Atom in Terminal Thiophene Ring

Keqiang He,[ab] Shujun Zhou,[c] Weili Li,[a] Hongkun Tian,[a] Qingxin Tang,*[d] Jidong Zhang,[a] Donghang Yan,[a] Yanhou Geng,*[aef] and Fosong Wang [a]*

[a]state Key Laboratory of Polymer Physics and Chemistry, Changchun Institute of Applied Chemistry, Chinese Academy of Sciences, Changchun 130022, P. R. China.
[b]University of Chinese Academy of Sciences, Beijing 100049, P. R. China.
[c]School of Mathematics and Physics, Bohai University, Jinzhou 121000, P. R. China
[d]Center for Advanced Optoelectronic Functional Materials Research and Key Laboratory of UV-Emitting Materials and Technology of Ministry of Education, Northeast Normal University, Changchun 130024, P. R. China.
[e]School of Materials Science and Engineering, Tianjin University, Tianjin 300072, P. R. China.
[f]Tianjin Key Laboratory of Molecular Optoelectronic Science and Collaborative Innovation Center of Chemical Science and Engineering (Tianjin), Tianjin 300072, P. R. China.

General Methods: ^{1}H NMR and ^{13}C NMR spectra were recorded on a Bruker AV 400-MHz spectrometer with $CDCl_3$ as solvent. Chemical shifts were reported as values (ppm) relative to internal tetramethylsilane. ^{13}C NMR spectra measurements for BTBTT6-syn and BTBTT6-anti were failed because of their insufficient solubility. Elemental analysis was carried out on a FlashEA1112 elemental analyzer. Matrix-assisted laser desorption ionization time-of-flight (MALDI-TOF) mass spectra were recorded in reflection mode on a Brucker/AutoflexIII mass spectrometer using dithranol (DIT) as the matrix. Density functional theory (DFT) calculations were carried out by using Gaussian 09 with a hybrid B3LYP correlation functional and 6-31G (d) basis set. TG-DTA was performed on a Perkin-Elmer TGA7 thermogravimetric analyzer at a heating rate of 10 °C min^{-1} in nitrogen. DSC measurements were carried out on a Perkin-Elmer DSC7 at a heating/cooling rate of 10/-10 °C min^{-1} at a nitrogen flow. Polarizing optical microscopic (POM) observation was performed on an Olympus BX51 polarizing optical microscope equipped with an LTS 350 hot stage and a TMS 94 temperature programmer (Linkam). UV-vis absorption spectra were measured on a Shimadzu UV3600 spectrometer. Fluorescence emission spectra were recorded on a Perkin-Elmer LS 50B luminescence spectrometer with Xenon discharge lamp excitation. Solution CV measurements of the isomers were carried out on a CHI660a electrochemical analyzer with a three electrode cell at a scan rate of 100 mV s^{-1} in dichloromethane (DCM) (10^{-3} mol L^{-1}) with Bu_4NPF_6 (0.1 mol L^{-1}) as electrolyte. A Pt disc electrode with a diameter of 2 mm, a Pt

wire, and a saturated calomel electrode were used as the working, counter and reference electrodes, respectively. The HOMO energy levels (E_{HOMO}) were calculated by the oxidation onset-potential versus ferrocene using the following equation: $E_{HOMO} = -(4.80 + E_{ox}^{onset})$ eV. Atomic force microscopy (AFM) measurements were carried out in a tapping mode on a SPA400HV instrument with a SPI 3800 controller (Seiko Instruments). Out-of-plane X-ray diffraction (XRD) was run on a Bruker D8 Discover thin-film diffractometer with CuKα radiation (λ= 1.54056 Å) performed at 40 kV and 40 mA in air. In-plane XRD was carried out on a Rigaku Smart Lab with CuKα source (λ = 1.54056 Å) in air.

Table S1. State-of-the-art mobilities of thienoacene-based molecules.

Compound	μ_{sat} ($cm^2V^{-1}s^{-1}$)	μ_{lin} ($cm^2V^{-1}s^{-1}$)	Processing method	ref
C_8-BTBT	16.4	N/A	Inkjet printing	1
C_{10}-DNTT	11	9	Edge-casting	2
DBTTT	19.3	N/A	Vacuum deposition	3
C_{13}-BTBT	17.2	N/A	Vacuum deposition	4
C10 -DNBDT-NW	16	N/A	Edge-casting	5
C6-DBTDT	18.9	N/A	Single-crystal	6
Ph-BTBT-10	13.9	N/A	Spin-coating	7
BTBT-T6	10.5	N/A	Vacuum deposition	8
BTBTT6-syn	11.7	10.6	Vacuum deposition	This work

Table S2. Crystallographic parameters of BTBTT6-syn and BTBTT6-anti.

	BTBTT6-syn	BTBTT6-anti
Chemical formula	$C_{22}H_{20}S_3$	$C_{22}H_{20}S_3$
Formula weight	380.56	380.56
Temperature/K	170	295
Wavelength/Å	1.34139	1.54178
Crystal system	Triclinic	Monoclinic
Space group	P $\bar{1}$	P 2_1/c
a/Å	9.7443(6)	20.4984(12)
b/Å	9.8799(6)	15.4320(10)
c/Å	40.142(3)	6.0388(4)
α/º	91.556(4)	90
β/º	92.432(3)	96.341(3)
γ/º	106.043(3)	90
V/Å^3	3707.6(4)	1898.6(2)
Z	8	4
D_{calc}/g·cm^{-3}	1.364	1.331
Absorption coefficient/mm^{-1}	2.375	3.561
F(000)	1600	800
Theta range for data collection/ º	4.055 to 55.16	3.593 to 67.495
Reflections collected	35703	12914
Independent reflections	13651 (R_{int}=0.0721)	3304 (R_{int}=0.0982)
Data completeness	0.955	0.966
Goodness of fit indicator	1.052	1.027
Final R indices [I > 2sigma(I)]	$R_1 = 0.1200$ $wR^2 = 0.3622$	$R_1 = 0.0794$ $wR^2 = 0.2059$
R indices (all data)	$R_1 = 0.1479$ $wR^2 = 0.3867$	$R_1 = 0.1117$ $wR^2 = 0.2190$
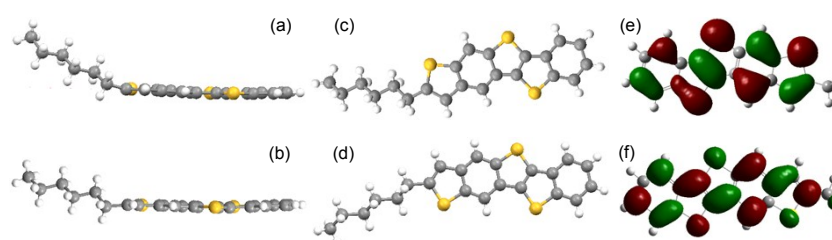
Figure S1. Geometries from single crystal analysis in side view (a, b) and top view (c, d) and DFT-optimized HOMOs (e, f) of BTBTT6-syn (a, c, e) and BTBTT6-anti (b, d, f). For the HOMOs, hexyl was replaced by methyl to simplify the calculations.
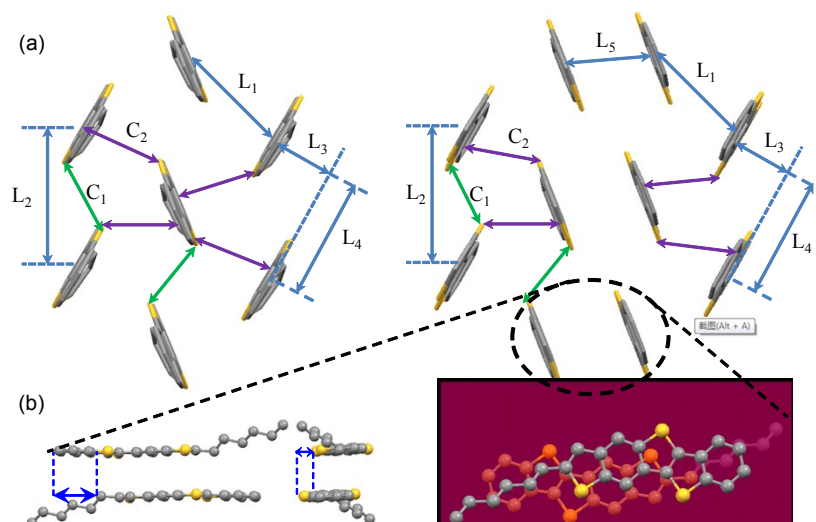
Figure S2. Sketch map of (a) structural parameters in herringbone (HB) packing of BTBTT6-syn (left) and sandwich-herringbone packing of BTBTT6-anti (right) and (b) slippage of anti-parallel dimer of BTBTT6-anti in π-π stacking.

Table S3. Parameters in HB packing of BTBTT6-syn and sandwich-HB packing of BTBTT6-anti.

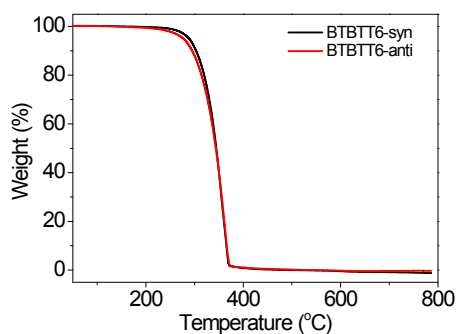|	BTBTT6-syn	BTBTT6-anti
Herringbone angle（°）	58.7	50.6
Intermolecular distance between the nearest T-shape contact molecules L_1（Å）	4.91−4.86	4.90
Centroid distances at the slipped parallel contacts L_2（Å）	5.88, 5.93	6.04
Interplanar distance L_3（Å）	2.58	2.57
Intermolecular slipped distance along short axis between the nearest parallel molecules L_4（Å）	5.28	5.46
Stacking distance between the parallel molecules L_5（Å）	--	3.64
Distance of S⋯S contacts C_1（Å）	3.48−3.56	3.50
Distance of S⋯C contacts C_2（Å）	3.38−3.43	3.46

Figure S3. TGA curves of BTBTT6-syn and BTBTT6-anti.

Table S4. Thermal properties of BTBTT6-syn and BTBTT6-anti from DSC curves.

	heating		cooling	
	BTBTT6-syn	BTBTT6-anti	BTBTT6-syn	BTBTT6-anti
T_L (°C)	248	221	--	--
T_1 (°C) / ΔH (J/g)	215/68.9	153/25.9	195/57.0	187/10.4
T_2 (°C) / ΔH (J/g)	--	159/5.8	186/11.7	124/34.3
T_3 (°C) / ΔH (J/g)	--	194/9.9	--	--
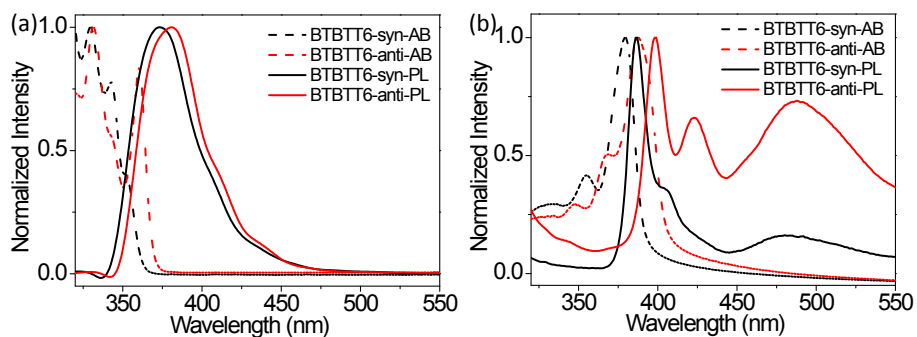
Figure S4. UV-vis absorption and PL spectra of BTBTT6-syn and BTBTT6-anti in DCM solutions with a concentration of 10^{-5} mol L^{-1} (a) and in the thin films vacuum deposited on the quartz substrates (b).
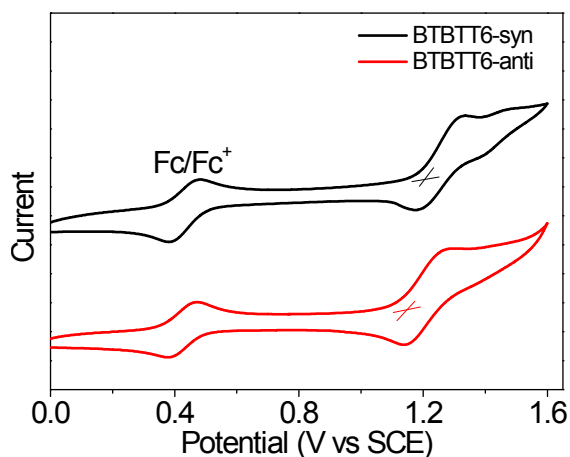
Figure S5. Solution cyclic voltammograms of BTBTT6-syn and BTBTT6-anti in dichloromethane (10^{-3} mol L^{-1}). The measurements were conducted at a scan rate of 50 mV s^{-1} with Bu_4NPF_6 (0.1 mol L^{-1}) as electrolyte and ferrocene as internal standard (E_{HOMO} = -4.80 eV). The HOMO energy levels were estimated by the onset of oxidation peaks *vs.* Fc/Fc$^+$, E_{HOMO} = -(4.80 + $E_{ox,onset}$).

Table S5. The HOMO energy levels of BTBTT6-syn and BTBTT6-anti.

	BTBTT6-syn	BTBTT6-anti	BTBT-T6
E_{HOMO} (eV)[a]	-5.35	-5.30	-5.31
E_{HOMO} (eV)[b]	-5.58	-5.52	-5.50

[a]obtained by DFT calculation; [b]obtained by CV measurement.

Table S6. OTFT device performance of BTBTT6-syn and BTBTT6-anti deposited on Sub$_{OTMS}$ without MoO_3 layers (Type I devices).

Compound	$\mu_{1\text{-ave}} \pm \sigma$ (cm^{2}V^{-1}s^{-1})	$\mu_{1\text{-max}}$ (cm^{2}V^{-1}s^{-1})	V_T (V)	$\mu_{2\text{-ave}} \pm \sigma$ (cm^{2}V^{-1}s^{-1})	$\mu_{2\text{-max}}$ (cm^{2}V^{-1}s^{-1})	V_T (V)	$I_{on/off}$
BTBTT6-syn	15.0 ±1.7	18.0	-21 - -23	9.6 ± 0.52	10.4	-9 - -14	10^7

device architecture: Au/ BTBTT6-syn/OTMS/SiO$_2$/Si; data were obtained from *ca.* 10 devices; T_S was 80 ^{o}C.
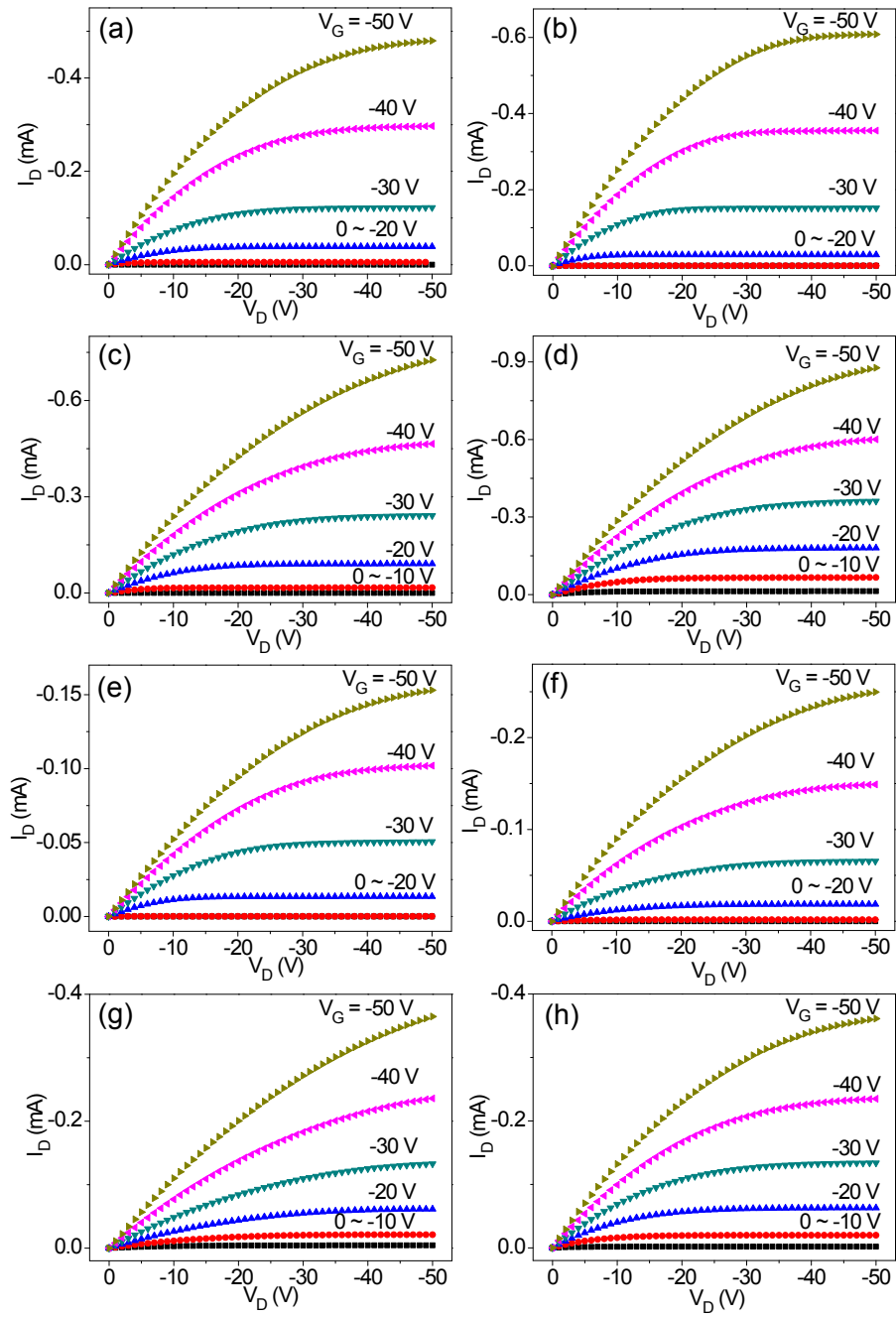
6

Figure S6. Typical output curves of Type I (a, e), II (b, f), III (c, g) and IV (d, h) devices based on BTBTT6-syn (a, b, c, d) and BTBTT6-anti (e, f, g, h).
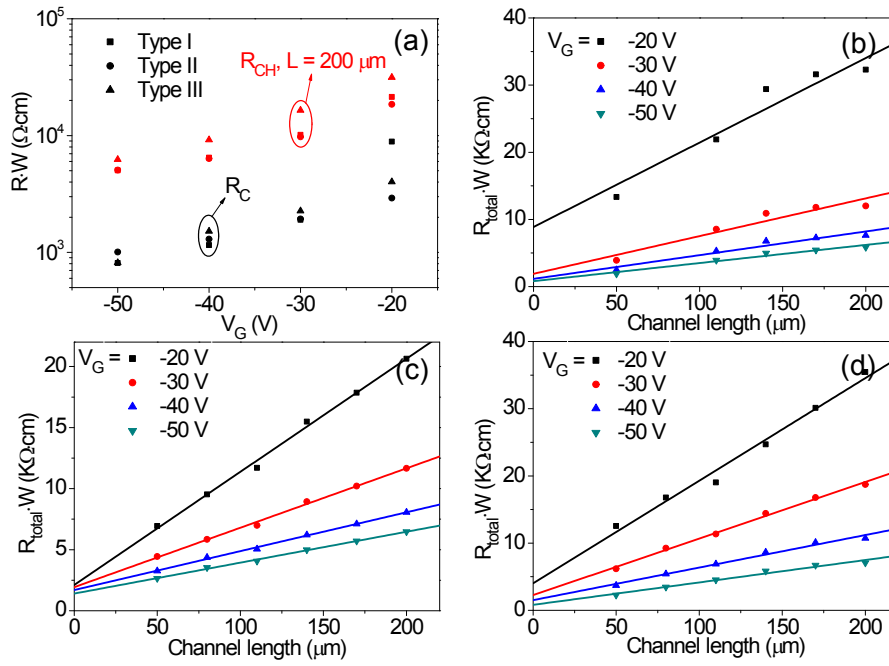
Figure S7. Width-normalized resistances (a) and TLM plots extracted from the TLM devices of BTBTT6-syn based on Type I (b), II (c) and III (d) devices.
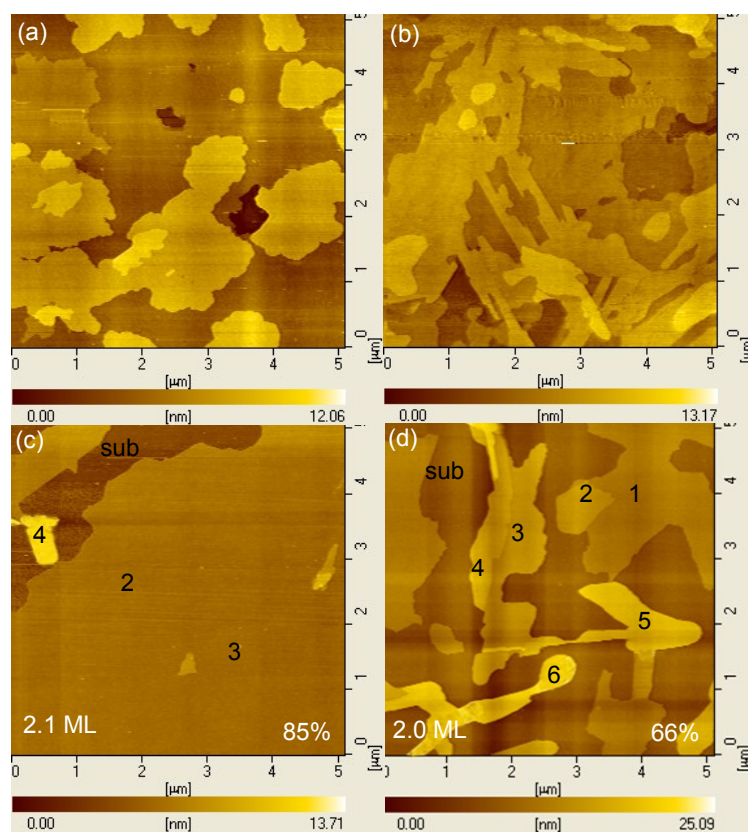
Figure S8. AFM height images (5 x 5 μm^2) of the thin films of BTBTT6-syn (a, c) and BTBTT6-anti (b, d) with thickness of 30 nm (a, b) and 5 nm (c, d) deposited on Sub$_{FDTES}$. In the images, the Arabic numerals represent the nominal thickness in terms of the number of corresponding molecular monolayers (ML). The percentage in the images (c, d) means coverage fraction of molecular layers.
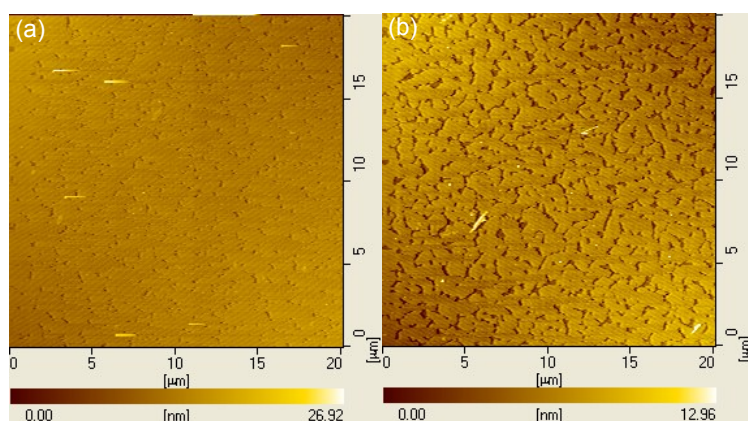

Figure S9. AFM height images (20 x 20 μm^2) of the films (5 nm) of BTBTT6-syn (a) and BTBTT6-anti (b) on Sub$_{OTMS}$.
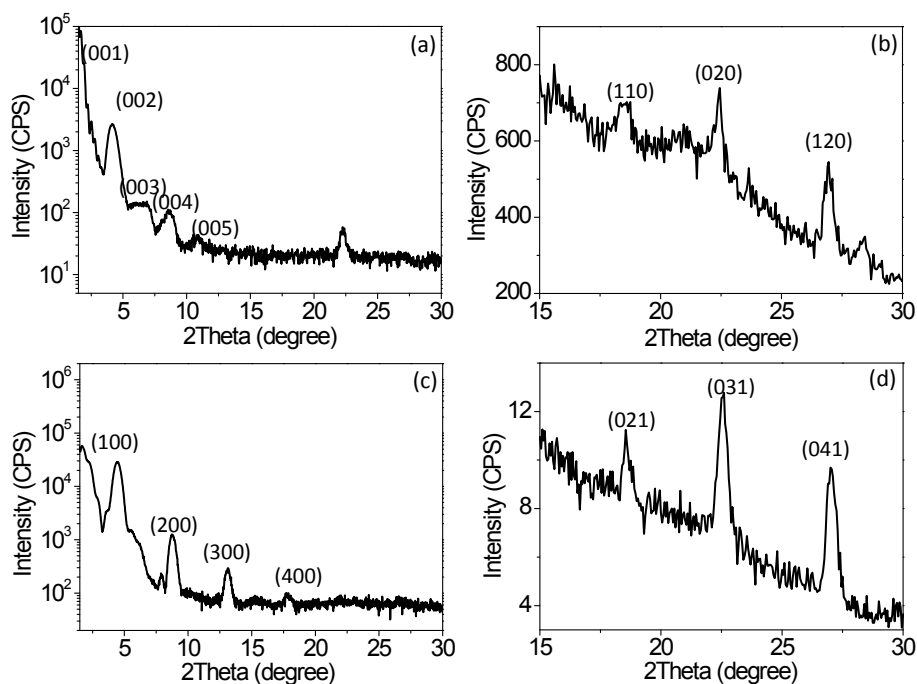
Figure S10. Out-of-plane (a, c) and in-plane XRD patterns (b, d) of thin films of BTBTT6-syn (a, b) and BTBTT6-anti (c, d) deposited on Sub$_{FDTES}$.

references

1 H. Minemawari, T. Yamada, H. Matsui, J. Tsutsumi, S. Haas, R. Chiba, R. Kumai and T. Hasegawa, *Nature*, 2011, **475**, 364-367.

2 K. Nakayama, Y. Hirose, J. Soeda, M. Yoshizumi, T. Uemura, M. Uno, W. Li, M. J. Kang, M. Yamagishi, Y. Okada, E. Miyazaki, Y. Nakazawa, A. Nakao, K. Takimiya and J. Takeya, *Adv. Mater.*, 2011, **23**, 1626-1629.

3 J. I. Park, J. W. Chung, J. Y. Kim, J. Lee, J. Y. Jung, B. Koo, B. L. Lee, S. W. Lee, Y. W. Jin and S. Y. Lee, *J. Am. Chem. Soc.*, 2015, **137**, 12175-12178.

4 A. Y. Amin, A. Khassanov, K. Reuter, T. Meyer-Friedrichsen and M. Halik, *J. Am. Chem. Soc.*, 2012, **134**, 16548-16550.

5 C. Mitsui, T. Okamoto, M. Yamagishi, J. Tsurumi, K. Yoshimoto, K. Nakahara, J. Soeda, Y. Hirose, H. Sato, A. Yamano, T. Uemura and J. Takeya, *Adv. Mater.*, 2014, **26**, 4546-4551.

6 P. He, Z. Tu, G. Zhao, Y. Zhen, H. Geng, Y. Yi, Z. Wang, H. Zhang, C. Xu, J. Liu, X. Lu, X. Fu, Q. Zhao, X. Zhang, D. Ji, L. Jiang, H. Dong and W. Hu, *Adv. Mater.*, 2015, **27**, 825-830.

7 H. Iino, T. Usui and J.-i Hanna, *Nat. Commun.*, 2015, **6**, 6828.

8 K. He, W. Li, H. Tian, J. Zhang, D. Yan, Y. Geng and F. Wang, *ACS Appl. Mater. Interfaces*, 2017, **9**, 35427-35426.